Self-Powered All-Inorganic Perovskite Photodetectors with Fast Response Speed

Ting Zhang
University of Electronic Science and Technology of China https://orcid.org/0000-0001-6385-6963
Shibin Li (shibinli@uestc.edu.cn)
University of Electronic Science and Technology of China

Nano Express

Keywords: CsPbI2Br, CsPbIBr2, anti-solvent processing, self-powered capability

Posted Date: November 18th, 2020

DOI: https://doi.org/10.21203/rs.3.rs-110344/v1

Version of Record: A version of this preprint was published on January 6th, 2021. See the published version at https://doi.org/10.1186/s11671-020-03460-4.

Abstract

In this manuscript, the inorganic perovskite $CsPbI_2Br$ and $CsPbIBr_2$ are investigated as photoactive materials that offers higher stability than the organometal trihalide perovskite materials. The fabrication methods allow anti-solvent processing the $CsPbI_xBr_{3-x}$ films, overcoming the poor film quality that always occur in a single-step solution process. The introduced diethyl ether in spin-coating process is demonstrated to be successful, and the effects of the anti-solvent on film quality are studied. The devices fabricated using the methods achieve a high-performance, self-powered and stabilized photodetectors with fast response speed. The results illustrate a great potential of all-inorganic $CsPbI_xBr_{3-x}$ perovskites in visible photodetection and provide an effective way to achieve high performance devices with self-powered capability.

Introduction

Photodetectors (PDs), which can convert light into electrical signal, are important applications in image, optical communication, and environmental monitoring. Conventional PDs are mainly made by Si, ZnO, SiC, and HgCdTe, which are either expensive or require vacuum equipment to fabricate [1–4]. Most importantly, these commercial devices usually need precise and complex fabrication process which combines lithography, etching and deposition, limiting a wide deployment [5, 6]. Therefore, it is of great interest to develop new materials for high performance photodetector via facile fabrication method.

Recently, organometal trihalide perovskites (OTPs) have emerged as an attractive class of optoelectronic materials due to their outstanding optoelectronic properties, such as strong light absorption, high carrier mobility, low exciton binding energy, and low charge recombination rate [7–12]. These features make OTPs as a promising photovoltaic material candidates for next generation solar cells. Indeed, since the emergence of perovskite-based solar cells (PSCs) in 2009 [13], certified power conversion efficiencies (PCEs) of organic-inorganic halide PSCs have rapidly increased to 25.2% [14]. Besides, OTPs have shown great potentials in PDs [15–17], light emitting diodes (LEDs) [18–20], and lasers [21–24]. Although continuous progress have been made in improving the efficiency, some opto-electronic devices based on OTPs still face a bottleneck of stability problem [25, 26]. Due to the degradation and volatilization of organic groups, such as methylammonium (MA^+) and formamidinium (FA^+) cations, OTPs suffers an unsatisfactory long-term stability [26]. Previous reported works demonstrate all-inorganic perovskites ($CsPbX_3$, X = I, Br, Cl) could solve the stability issue probably because of their intrinsic chemical stability [27–29]. Among these all-inorganic perovksites, black phase $CsPbI_3$ has garnered great interest due to its suitable bandgap of 1.7 eV. Unfortunately, black-$CsPbI_3$ is only stable at temperatures above 330℃, which is not practical for applications [27]. Partially replacing iodide with bromide can stabilize the black phase of all-inorganic perovskites at room temperature and would not trade off the optical bandgap too much [30–32]. Recently, there are too many researches on $CsPbI_xBr_{3-x}$ perovskite solar cells, less works about PDs based on $CsPbI_xBr_{3-x}$ thin films have been reported. Moreover, the traditional PDs generally need external power sources to drive photogenerated carriers to input photocurrent. To meet the demands

of next generated opto-electronic devices aimed at reduced weight, size and thickness, it is urgent to develop effective methods for the fabrication of PDs with self-powered capability.

Herein, we report high performance perovskite photodetectors based on solution-processed all-inorganic $CsPbI_xBr_{3-x}$ perovskite. At a low operation voltage of 2 V, the detectors showed broadband sensitivity covering visible light spectrum and fast response speed down to 175 μs for $CsPbI_2Br$ PDs and 230 μs for $CsPbIBr_2$ PDs. The detectivity and on/off ratio were calculated to be 10^{11} Jones and 10^3, respectively. Even biased at 0 V, both the devices still worked well. This work provides a sample method to fabricate high-performance photodetectors in visible light with self-powered capability.

Method

Materials

Barium iodide (CsI, 99.9%), lead iodide (PbI_2, 99.99%), barium bromide (CsBr, 99.99%) and lead bromide ($PbBr_2$, 99.99%) were purchased from Xi'an Polymer Light Technology Corporation. Anhydrous dimethylformamide (DMF), dimethyl sulfoxide (DMSO) and diethyl ether (DEE) were purchased from Sigma-Aldrich Corporation. Materials and solvents were used directly without purification.

The all-inorganic perovskite films were fabricated by one-step method using anti-solvent. First, to obtain the $CsPbI_xBr_{3-x}$ (x = 1, 2) precursor solution, stoichiometric-ratio PbI_2, CsI, CsBr and $PbBr_2$ were dissolved in a mixed solvent of DMF and DMSO (9:1 v/v) at 1.43M and stirred for more than 2 h. All of the procedures should be operated in a nitrogen filled glovebox.

Preparation

ITO-coated glass substrates were cleaned by acetone, ethyl alcohol and deionized water with each step for 15 min and dried in an oven. To form perovskite films, the precursor was spin-coated on pre-cleaned ITO substrates at a speed of 2000 rpm for 60 s, and dropped 500 μL antisolvent diethyl ether (DEE, Sigma, 99.9%) at the last 20 s of the coating process. Then the perovskite films were annealed at 65 ℃ for 5 min and 135 ℃ for 15 min. To compare the film-quality enhanced by anti-solvent DEE, reference experiment, of which no antisolvent was introduced, also been conducted. Finally, 80 nm thick interdigitated Au electrodes were thermally evaporated on perovskite films via mask.

Measurements and Characterizations

The morphologies of as-prepared films were investigated by field emission scanning electron microscopy (FE-SEM). The phases and crystalline of as-synthesized inorganic perovskite were recorded by X-ray diffraction (XRD) patterns using an X-ray diffractometer (Cu Kα radiation, λ = 1.54056 Å). The UV-Vis absorption and PL spectra were performed using a UV-Vis spectrophotometer (Shimadzu UV-3101 PC) and a Hitachi F-4600 fluorescence spectrometer (Edinburgh, FLSP920) with an exciting wavelength of 410 nm, respectively. The current-voltage (I-V) curves were recorded by a Keithley 4200 Semiconductor Parametric Analyzer under the illumination of a LD light source (520 nm). The incident light intensity was

measured by a commercial power meter with the type of Thorlabs PM 100D. Photocurrent and response speed were measured with an oscilloscope (Agilent DOS5012A) and an optical chopper modulating the light illuminated on the device. All the measurements were conducted in air atmosphere at room temperature.

Results And Discussion

Figure 1 shows the top-view SEM images of $CsPbI_2Br$ and $CsPbIBr_2$ thin films with or without anti-solvent DEE treatment. Obviously, the pristine $CsPbI_xBr_{3-x}$ perovskite films are discontinuous and shows large pinholes. After DEE treatment, the film quality of $CsPbI_xBr_{3-x}$ are significantly enhanced showing higher coverage and compactness. To further investigate the crystal structure and phase purity of all-inorganic perovskite films, XRD patterns were recorded as displayed in Figure 2a. For the pattern of $CsPbI_2Br$ film, the main peaks at 14.6° and 29.6° are assigned to the (100) and (200) crystallographic planes of the $CsPbI_2Br$ cubic perovskite structure, respectively. For the case of $CsPbIBr_2$ film, the three peaks centered at 14.9°, 21.08° and 29.96° are associated with the (100), (110) and (220) planes of the $CsPbIBr_2$ perovskite orthorhombic phase, respectively. In addition, the ratios of diffraction peak (P) 14.6° and 29.6° are calculated to be 1.10 and 1.12 for $CsPbI_2Br$ after DEE treatment, respectively. This indicates that the $CsPbI_2Br$ perovskite film grow preferentially with (200) facet on DEE treatment. Meanwhile, for the case of $CsPbIBr_2$ perovskite film after DEE treatment, the ratios of diffraction peak (P) 14.9° and 29.96° are calculated to be 5 and 12, respectively, which demonstrates the $CsPbIBr_2$ perovskite film grow preferentially with (200) facet on DEE treatment. Both the XRD results demonstrate that the DEE treatment can improve the crystalline quality and phase purity of $CsPbI_xBr_{3-x}$ films obviously.

Furthermore, the optical properties of $CsPbI_xBr_{3-x}$ films with or without DEE treatment were measured by UV-Vis absorption and PL spectrum. As shown in Figure 2b, both $CsPbI_2Br$ and $CsPbIBr_2$ samples present an improved absorbance after DEE treatment. The absorbance spectra suggest these $CsPbI_xBr_{3-x}$ films can be used as an active layer for visible photodetection effectively. Figure 2c is the PL spectra of $CsPbI_2Br$ and $CsPbIBr_2$ films deposited on SnO_2 substrates. The PL peak located at 655 nm and 603 nm, respectively, which were in agreement with the previous reports. For the cases treated by DEE, the PL intensity was reduced significantly compared to that of untreated perovskite films. The reduced PL intensity related to the decreased trap density which would facilitate carriers in the excited state recombination to the ground radiatively. The results indicate that introducing the DEE anti-solvent is an effective way to achieve better film quality and reduction of trap density in all-inorganic perovskite films. Therefore, we used the modified perovskite films as photoactive layers to fabricate all-inorganic $CsPbI_xBr_{3-x}$ perovskite PDs, with the structure shown in Figure 3a.

Figure 3b shows the I-V curves of the devices in dark and under 520 nm light illumination. Under the illumination of 520 nm light source, the photocurrent was increased greatly due to the large contribution from the photogenerated carriers. Obviously, the photocurrent curves of two different PDs show a rectification behavior, indicating that junction barriers exist between the ITO and perovskite films. These

junction barriers could be ascribed to Schottky contact formed at the ITO/$CsPbI_2Br$ or ITO/$CsPbIBr_2$ interface and the surface states, such as surface defects, vacancies and absorption [33]. The phenomenon always exists in previously reported perovskite PDs [34-36]. When the device was biased at 0.1 V, the detector based on $CsPbI_2Br$ perovskite showed a dark current of ~2 nA. Once exposed to a 520 nm laser diode (LD) light source with the illumination intensity of 3.5 mW/cm^2, the photocurrent increased to μA, achieving a high on/off ratio larger than 10^3. For the case of $CsPbIBr_2$ photodetector biased at 0.1 V, the dark current was 2.45 nA, which resulted in an on/off ratio of 10^3 as well. When the light source was switched on and off, both the devices showed a rapid response in the current-time (I-t) curves at zero bias, as displayed in Figure 3c and d. When light was on, the photocurrent increased sharply and then decreased rapidly once the light was turn off. It is noted that I-t curves were measured by controlling the LD light source to achieve on/off recycles. The results further illustrated that the $CsPbI_xBr_{3-x}$ perovskite photodetectors showed a good light-switching behavior and reproducible photocurrent response to periodic on/off light. In addition, the I-t curves fit well with the I-V curves, further illustrating the devices have fast response speed and lower delaying properties. As the critical parameters for evaluating a commercial photodetector, responsivity (R) and specific detectivity (D) are analyzed. When the dark current is assumed to be dominated by shot noise, D can be calculated by the following equation

$$D^* = \frac{J_{ph}}{L_{light}} \frac{1}{(2qJ_d)^{1/2}} = \frac{R}{(2qJ_d)^{1/2}}$$

Where J_d is the dark current, J_{ph} is the photocurrent, L_{light} is the incident light intensity. R means the photocurrent generated per unit intensity of the incident light, which reflects the efficiency of the detector responds to the incident light signals.

Figure 4a and b show the detectivity and responsivity values of $CsPbI_2Br$ and $CsPbIBr_2$ perovskite photodetectors measured at different incident light power. For $CsPbI_2Br$ device, under weak (3.5 mW/cm^2) and strong (6 mW/cm^2) illumination, D* were calculated to be 4.9×10^{11} and 3.2×10^{11} Jones ( ), respectively. For the case of $CsPbIBr_2$ photodetector, D* under weak and strong light illumination were ~2.3×10^{11} and 1.3×10^{11} Jones, respectively. The calculated D* and R values decreased linearly with the increase of incident light intensity. Under strong illumination (6 mW/cm^2), the $CsPbI_2Br$ and $CsPbIBr_2$ detectors showed R values of 8 mA/W and 4.6 mA/W, respectively. Under weak illumination (3.5 mW/cm^2), both the above-mentioned PDs showed good performance with R of 12 and 8 mA/W, respectively. The high detectivity means the weak light signals also could be detected and transferred into large photocurrent. This is attributed to the improved all-inorganic perovskite film quality via DEE treatment.

Further, the response speed is a figure-of-merit for photodetectors to characterize the device. We defined the rise time as the time spent on rising from 10% to 90% of maximum photocurrent, and vice versa

means the decay time. To obtain the detailed response speed, an oscilloscope was used to control and record the temporal response. As plotted in Figure 5a and b, the rise time and decay time for $CsPbI_2Br$ device were extracted to be 175 and 180 μs. Meanwhile, the rise and decay time for $CsPbIBr_2$ were 320 and 230 μs, respectively. The fast response time means less electronic trap states exist at the interface of perovskite/metal, which could affect the charge transport and collection.

In summary, we reported the facile fabrication of self-powered all-inorganic $CsPbI_xBr_{3-x}$ PDs with fast response speed. Under 520 nm laser illumination with 3.5 mW/cm^2, the $CsPbI_2Br$ devices showed a responsivity up to 12 mA/W, detectivity values of 10^{11} Jones, on/off ratios larger than 10^3. And the $CsPbIBr_2$ devices showed a responsivity values of 8 mA/W and detectivity up to 10^{11} Jones. The devices can work well even at zero bias. This work inspires the development of all-inorganic perovskite for solution-processed, self-powered and high performance photodetectors.

Declarations

Acknowledgements

This work was supported by the National Natural Science Foundation of China (61874150), the Sichuan Key Project for Applied Fundamental Research (20YYJC4341) and the Key Laboratory Foundation of Chinese Academy of Sciences

(2019LBC).

Contributions

TZ designed and conducted the experiments, analyzed the data and prepared the manuscript. SL has given the final approval of the version to be published. All authors read and approved the final manuscript.

Funding

National Natural Science Foundation of China (61874150), Sichuan Key Project for Applied Fundamental Research (20YYJC4341) and the Key Laboratory Foundation of Chinese Academy of Sciences (2019LBC).

Availability of Data and Materials

The data generated or analyzed during the current study are obtained from the corresponding author on reasonable request.

Abbresviations

PDs: Photodetectors; OTPs: Organometal trihalide perovskites; DEE: Diethyl ether; DMF: Dimethylformamide; DMSO: Dimethyl sulfoxide; SEM: Scanning electron microscope; UV-Vis: Ultraviolet-visible; XRD: X-ray diffraction

Competing Interests

The authors declare that they have no competing interests.

References

[1] Zhang T, Liu B, Ahmad W et al (2017) Optical and electronic properties of femtosecond laser-induced sulfur-hyperdoped silicon N^+/P photodiodes. Nanoscale Res Lett 12(1): 1-4

[2] Jin Y, Wang J, Sun B et al (2008) Solution-processed ultraviolet photodetectors based on colloidal ZnO nanoparticles. Nano Lett 8(6): 1649-1653

[3] Chen X, Zhu H, Cai J et al (2007) High-performance 4H-SiC-based ultraviolet p-i-n photodetector. J Appl Phys 102(2): 024505

[4] Tennant W E (2012) Interpreting mid-wave infrared MWIR HgCdTe photodetectors. Prog Quantum Electron 36(2-3): 273-292

[5] Gong X, Tong M, Xia Y et al (2009) High-detectivity polymer photodetectors with spectral response from 300 nm to 1450 nm. Science 325(5948): 1665-1667

[6] Baeg K J, Binda M, Natali D et al (2013) Organic light detectors: photodiodes and phototransistors. Adv Mater 25(31): 4267-4295

[7] Li S, Zhang P, Wang Y et al (2017) Interface engineering of high efficiency perovskite solar cells based on ZnO nanorods using atomic layer deposition. Nano Res 10(3): 1092-1103

[8] Leijtens T, Stranks S D, Eperon G E et al (2014) Electronic properties of meso-superstructured and planar organometal halide perovskite films: charge trapping, photodoping, and carrier mobility. ACS Nano 8(7): 7147-7155

[9] Dursun I, Zheng Y, Guo T et al (2018) Efficient photon recycling and radiation trapping in cesium lead halide perovskite waveguides. ACS Energy Lett 3(7): 1492-1498

[10] De Wolf S, Holovsky J, Moon S J et al (2014) Organometallic halide perovskites: sharp optical absorption edge and its relation to photovoltaic performance. J Phys Chem Lett 5(6): 1035-1039

[11] Miyata A, Mitioglu A, Plochocka P et al (2015) Direct measurement of the exciton binding energy and effective masses for charge carriers in organic–inorganic tri-halide perovskites. Nat Phys 11(7): 582-587

[12] Wehrenfennig C, Eperon G E, Johnston M B (2014) High charge carrier mobilities and lifetimes in organolead trihalide perovskites. Adv Mater 26(10): 1584-1589

[13] Kojima A, Teshima K, Shirai Y (2009) Organometal halide perovskites as visible-light sensitizers for photovoltaic cells. J Am Chem Soc 131(17): 6050-6051

[14] http://www.nrel.gov/pv/assets/images/efficiency-chart.gnp [OL]

[15] Saidaminov MI, Adinolfi V, Comin R et al (2015) Planar-integrated single-crystalline perovskite photodetectors. Nat Commun 6(1)：1-7

[16] Dou L, Yang Y, You J, et al (2014) Solution-processed hybrid perovskite photodetectors with high detectivity. Nat Commun 5(1)：1-6

[17] de Arquer FPG, Armin A, Meredith P, et al (2017) Solution-processed semiconductors for next-generation photodetectors. Nat Rev Mater 2(3): 1-17

[18] Wang N, Cheng L, Ge R et al (2016) Perovskite light-emitting diodes based on solution-processed self-organized multiple quantum wells. Nat Photonics 10(11): 699-704

[19] Zou W, Li R, Zhang S et al (2018) Minimising efficiency roll-off in high-brightness perovskite light-emitting diodes. Nat Commun 9(1): 1-7

[20] Lin K, Xing J, Quan LN et al (2018) Perovskite light-emitting diodes with external quantum efficiency exceeding 20 per cent. Nature 562(7726): 245-248

[21] Liu P, He X, Ren J et al (2017) Organic–inorganic hybrid perovskite nanowire laser arrays. ACS Nano 11(6): 5766-5773

[22] Sutherland BR, Sargent EH (2016) Perovskite photonic sources. Nat Photonics 10(5): 295

[23] Tang X, Hu Z, Yuan W (2017) Perovskite $CsPb_2Br_5$ microplate laser with enhanced stability and tunable properties. Adv Opt Mater 5(3): 1600788

[24] Shang Q, Li M, Zhao L et al (2020) Role of the exciton–polariton in a continuous-wave optically pumped $CsPbBr_3$ perovskite laser. Nano Lett 20(9): 6636-6643

[25] Niu G, Guo X, Wang L (2015) Review of recent progress in chemical stability of perovskite solar cells. J Mater Chem A 3(17): 8970-8980

[26] Domanski K, Correa-Baena JP, Mine N (2016) Not all that glitters is gold: metal-migration-induced degradation in perovskite solar cells. ACS Nano 10(6): 6306-6314

[27] Zhang T, Wang F, Chen H et al (2020) Mediator–Antisolvent Strategy to Stabilize All-Inorganic CsPbI3 for Perovskite Solar Cells with Efficiency Exceeding 16%. ACS Energy Lett 5(5): 1619-1627

[28] Zhang T, Wang F, Zhang P et al (2019) Low-temperature processed inorganic perovskites for flexible detectors with a broadband photoresponse. Nanoscale 11(6): 2871-2877

[29] Xiang W, Tress W (2019) Review on recent progress of all-inorganic metal halide perovskites and solar cells. Adv Mater 31(44): 190285

[30] Chen W, Chen H, Xu G et al (2019) Precise control of crystal growth for highly efficient $CsPbI_2Br$ perovskite solar cells. Joule 3(1): 191-204

[31] Zhang J, Bai D, Jin Z et al (2018) 3D–2D–0D interface profiling for record efficiency all-inorganic $CsPbBrI_2$ perovskite solar cells with superior stability. Adv Energy Mater 8(15): 1703246

[32] Yan L, Xue Q, Liu M et al (2018) Interface engineering for all-inorganic $CsPbI_2Br$ perovskite solar cells with efficiency over 14%. Adv Mater 30(33): 1802509

[33] Kind H, Yan H, Messer B et al (2002) Nanowire ultraviolet photodetectors and optical switches. Adv Mater 14(2): 158-160

[34] Zhang T, Wu J, Zhang P et al (2018) High Speed and stable solution-processed triple cation perovskite photodetectors. Adv Opt Mater 6(13): 1701341

[35] Shaikh PA, Shi D, Retamal JRD et al (2016) Schottky junctions on perovskite single crystals: light-modulated dielectric constant and self-biased photodetection. J Mater Chem C 4(35): 8304-8312

[36] Guan X, Hu W, Haque M A et al [2018] Light-responsive ion-redistribution-induced resistive switching in hybrid perovskite Schottky junctions. Adv Funct Mater 28(3): 1704665

Figures

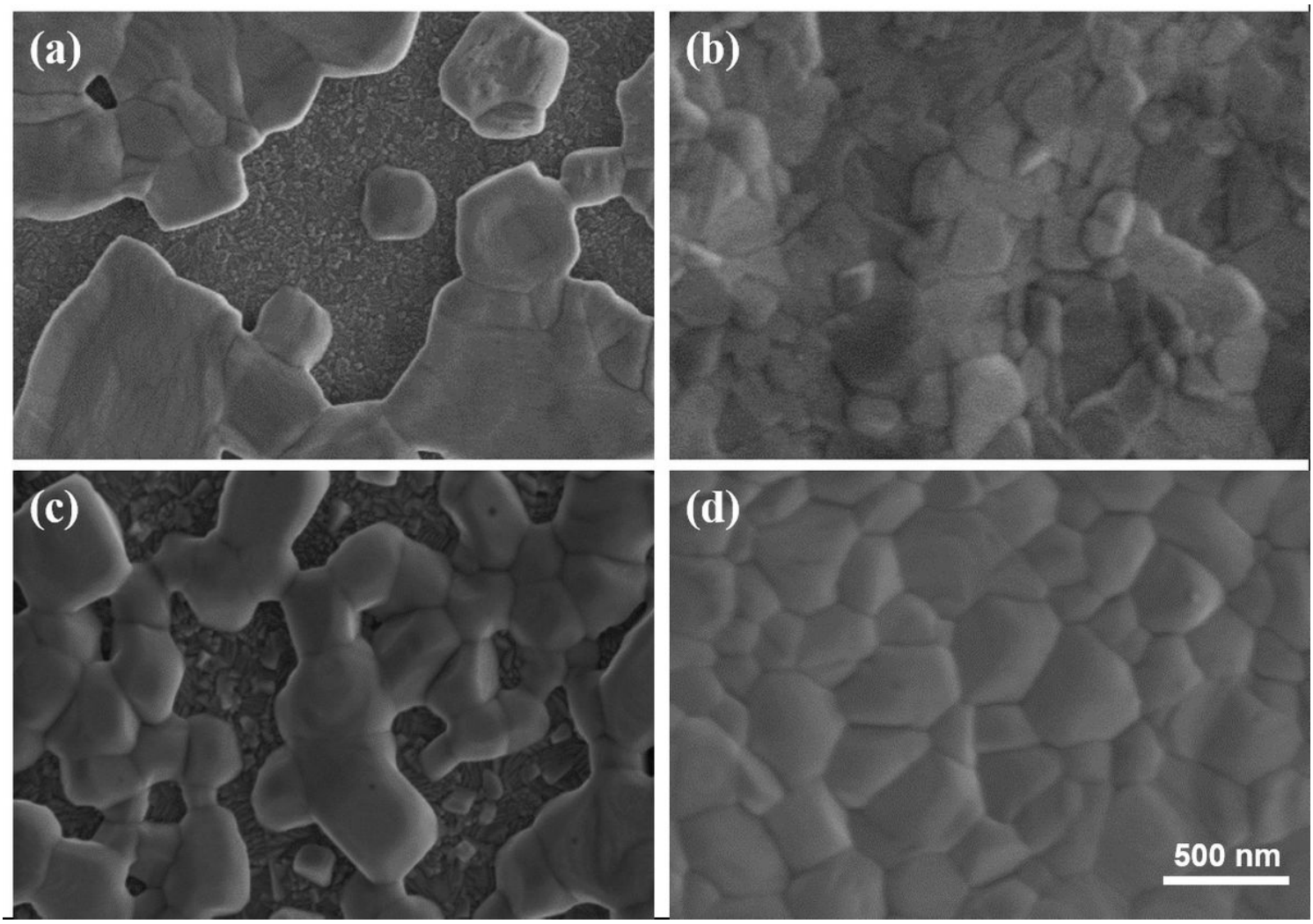

Figure 1

Top-view SEM images of the all-inorganic perovskite films. CsPbI2Br film a without b with DEE treatment; CsPbIBr2 films c without d with DEE treatment.

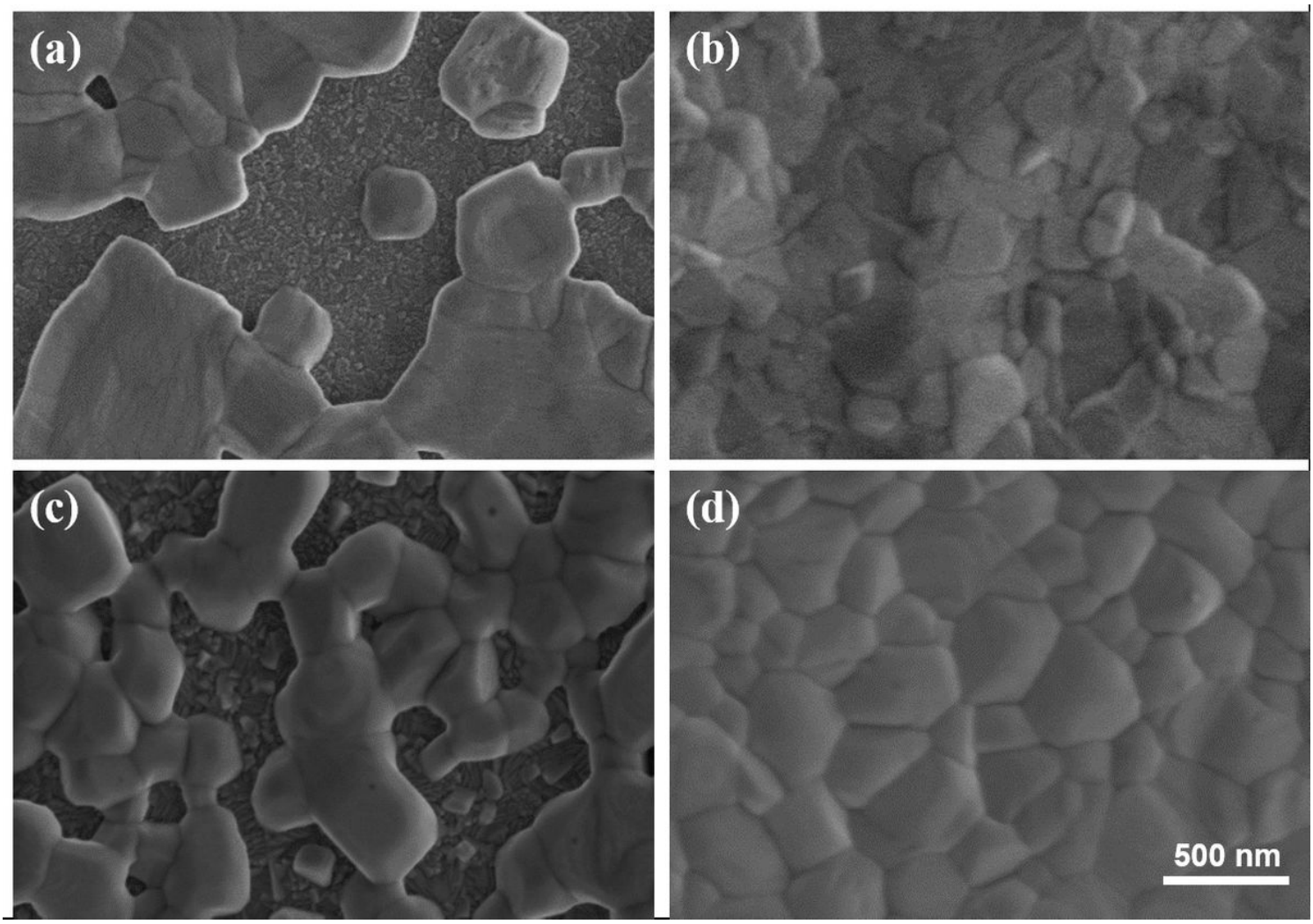

Figure 1

Top-view SEM images of the all-inorganic perovskite films. CsPbI2Br film a without b with DEE treatment; CsPbIBr2 films c without d with DEE treatment.

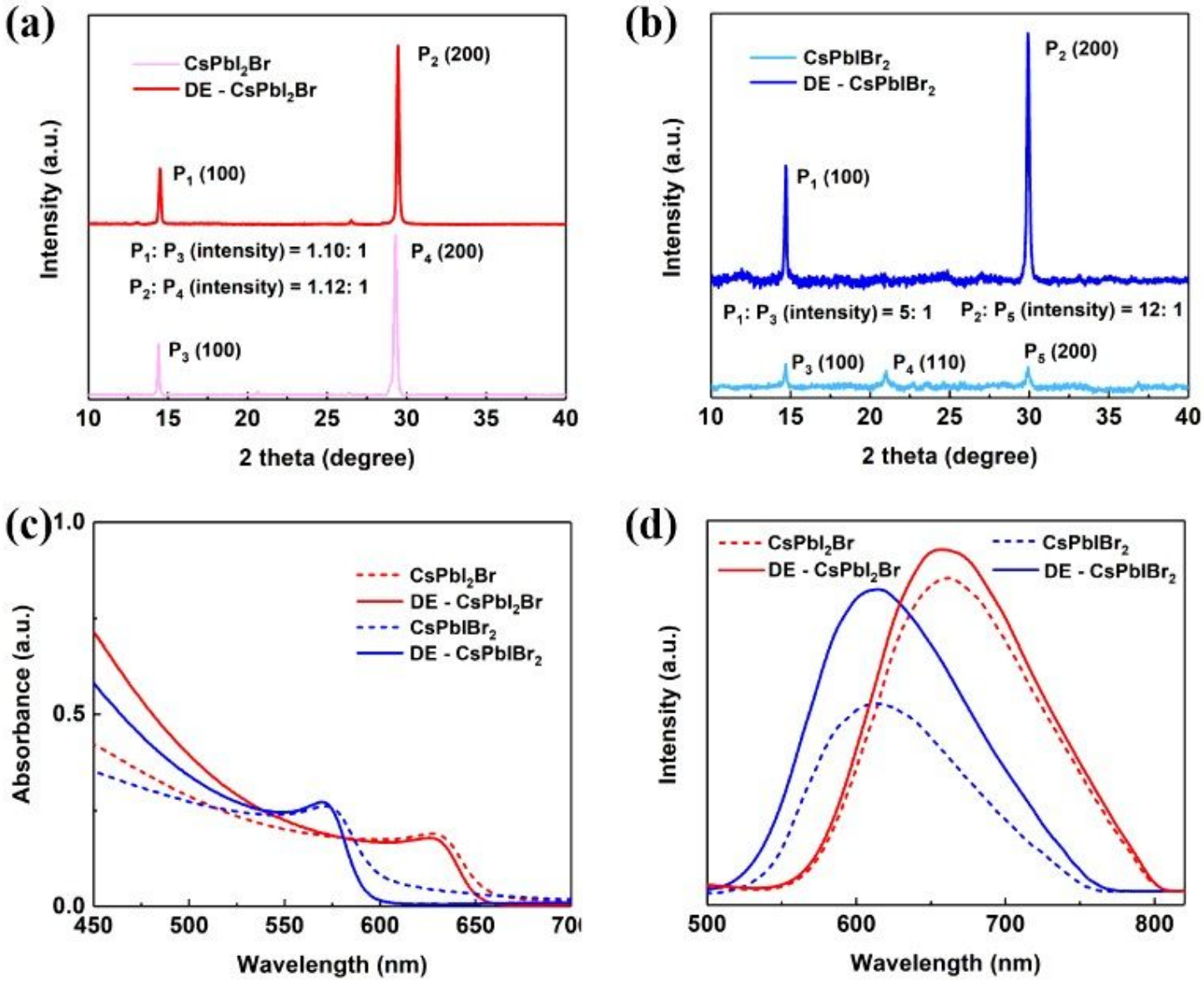

Figure 2

Comparison of a XRD patterns of CsPbI2Br films, b XRD patterns of CsPbIBr2, c absorption of CsPbIxBr3-x, d photoluminiescence spectra of CsPbIxBr3-x with or without DEE treatment.

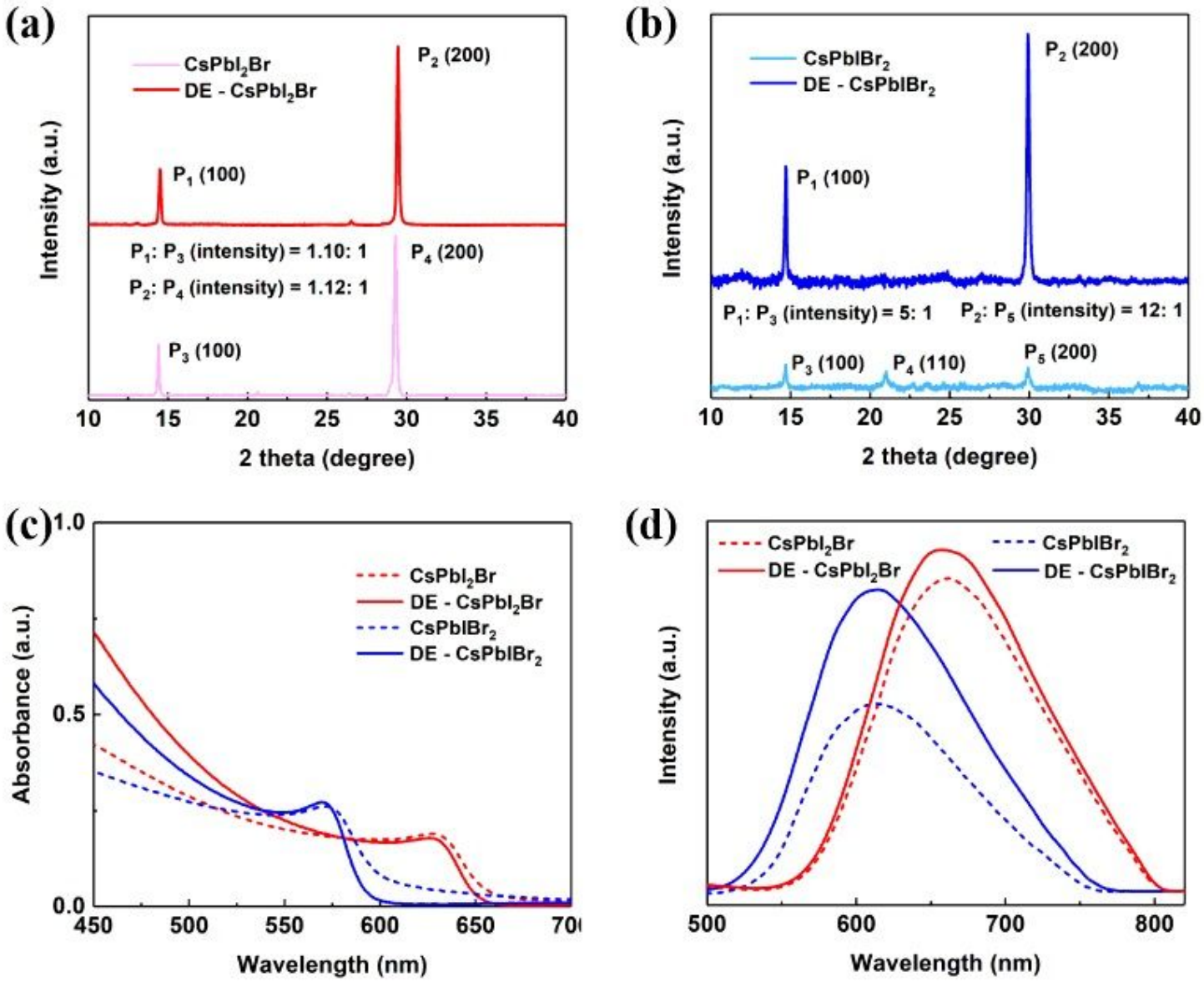

Figure 2

Comparison of a XRD patterns of CsPbI2Br films, b XRD patterns of CsPbIBr2, c absorption of CsPbIxBr3-x, d photoluminiescence spectra of CsPbIxBr3-x with or without DEE treatment.

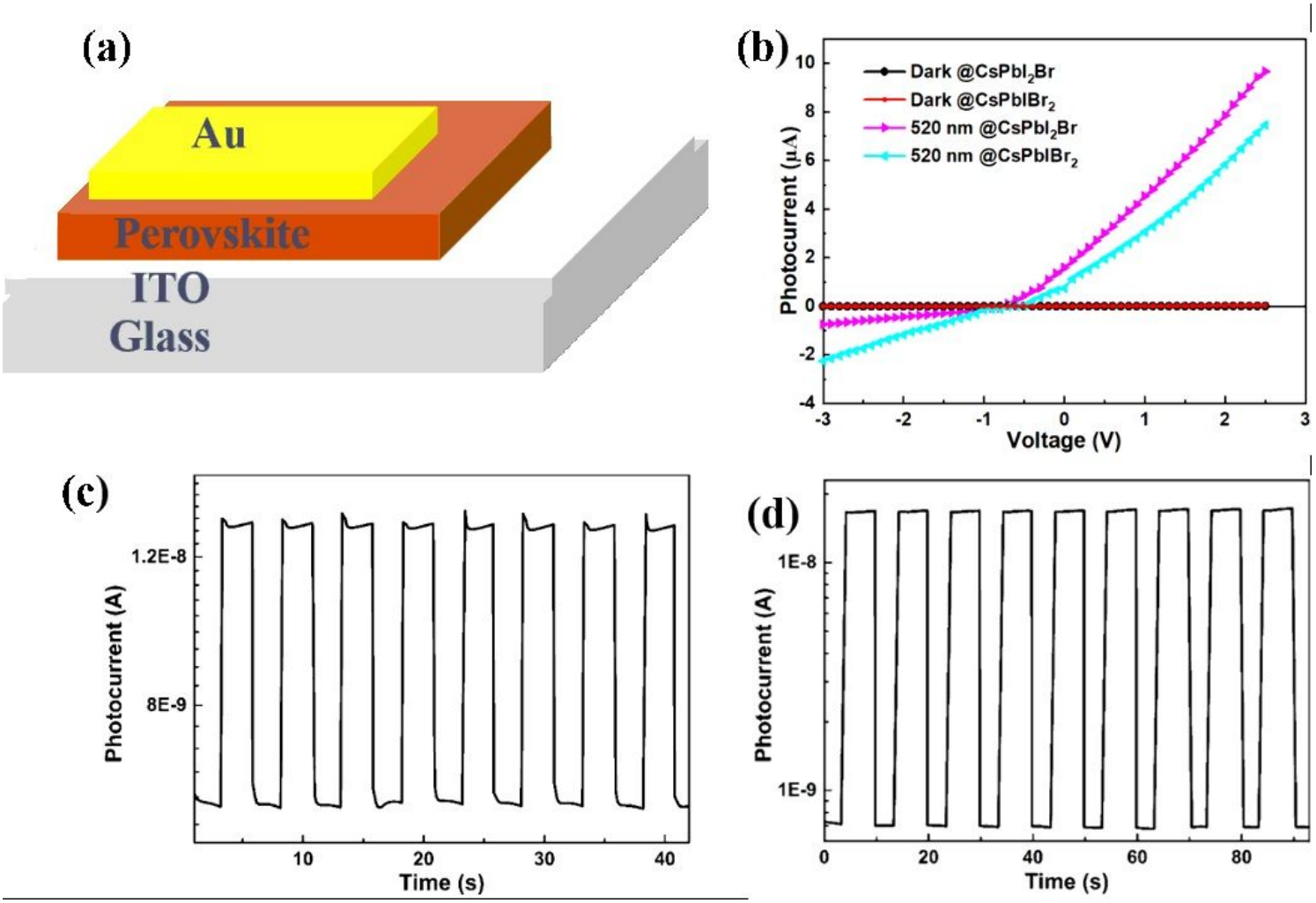

Figure 3

Optoelectronic performance of CsPbIxBr3-x perovskite PDs. a schematic illustration of the CsPbIxBr3-x perovskite photodetector, b current-voltage characteristics of the CsPbIxBr3-x perovskite PDs in the dark and under 520 nm illumination with light intensity of 3.5 mW/cm2, c temporal photoresponse of the CsPbI2Br PDs under 520 nm irradiation when biased at 0 V, d I-t curve of the CsPbI2Br PDs under 520 nm irradiation at 0 V.

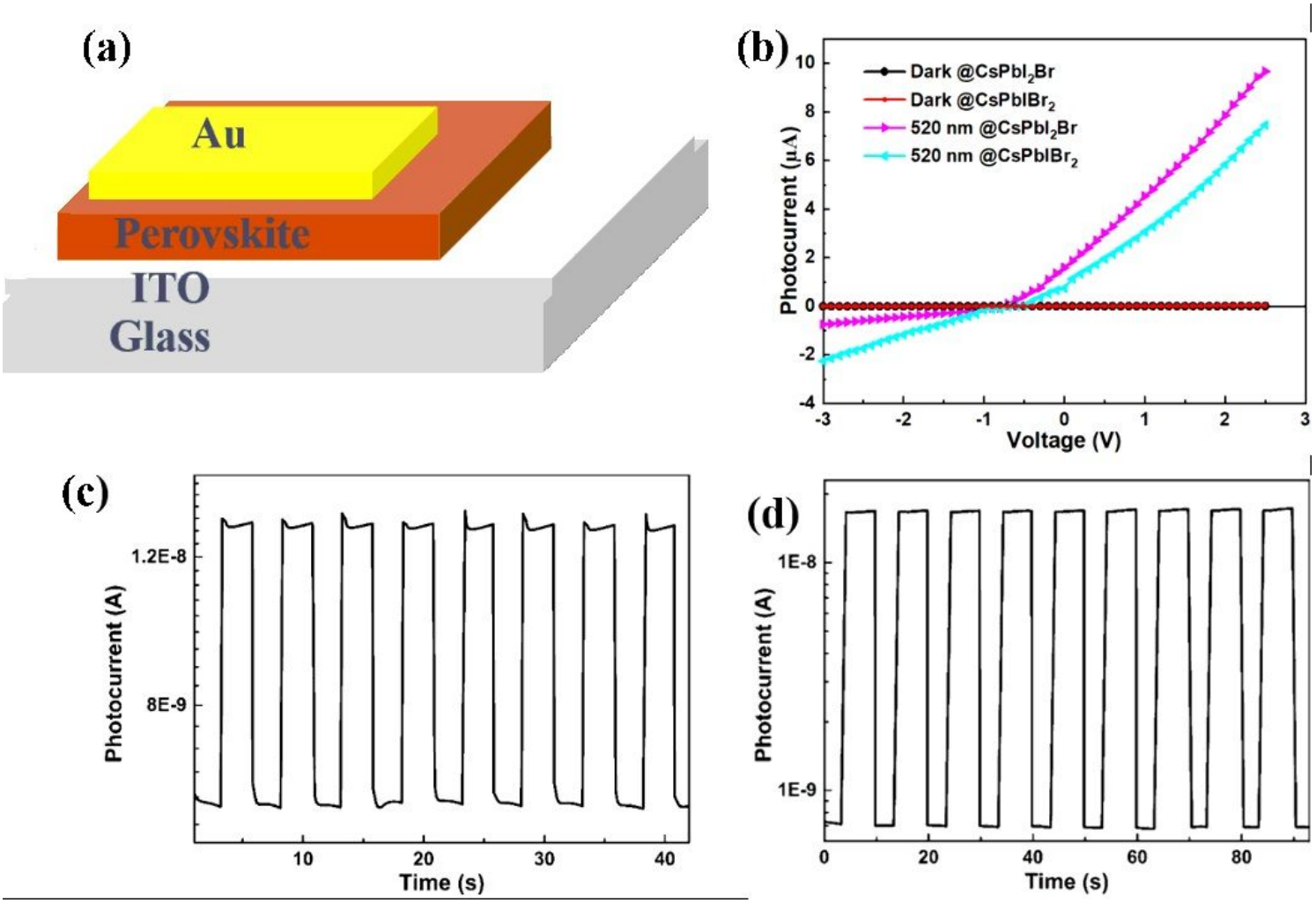

Figure 3

Optoelectronic performance of CsPbIxBr3-x perovskite PDs. a schematic illustration of the CsPbIxBr3-x perovskite photodetector, b current-voltage characteristics of the CsPbIxBr3-x perovskite PDs in the dark and under 520 nm illumination with light intensity of 3.5 mW/cm2, c temporal photoresponse of the CsPbI2Br PDs under 520 nm irradiation when biased at 0 V, d I-t curve of the CsPbI2Br PDs under 520 nm irradiation at 0 V.

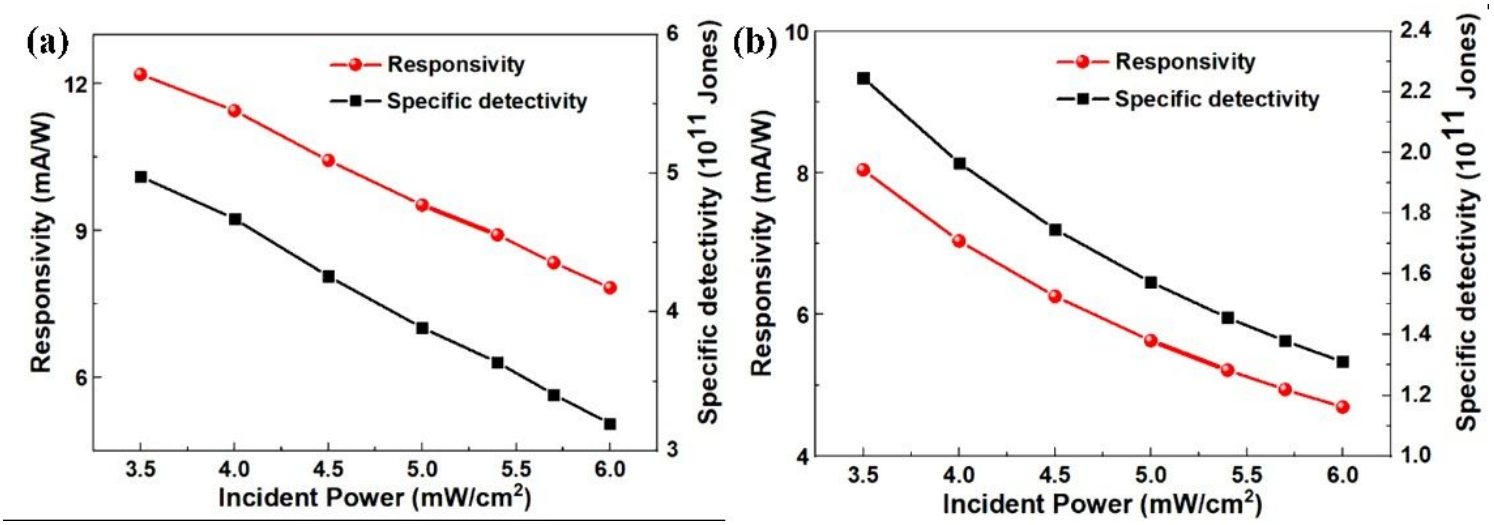

Figure 4

Responsivity and specific detectivity of CsPbIxBr3-x perovskite PDs. a CsPbI2Br perovskite photodetector, b CsPbIBr2 perovskite photodetector.

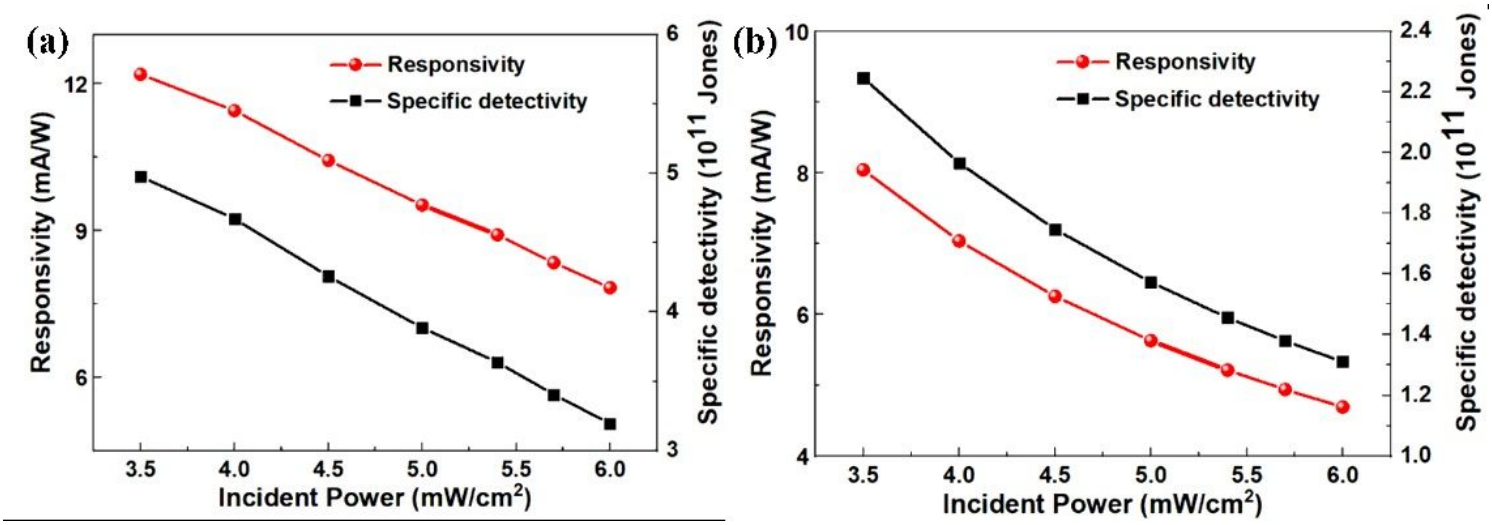

Figure 4

Responsivity and specific detectivity of CsPbIxBr3-x perovskite PDs. a CsPbI2Br perovskite photodetector, b CsPbIBr2 perovskite photodetector.

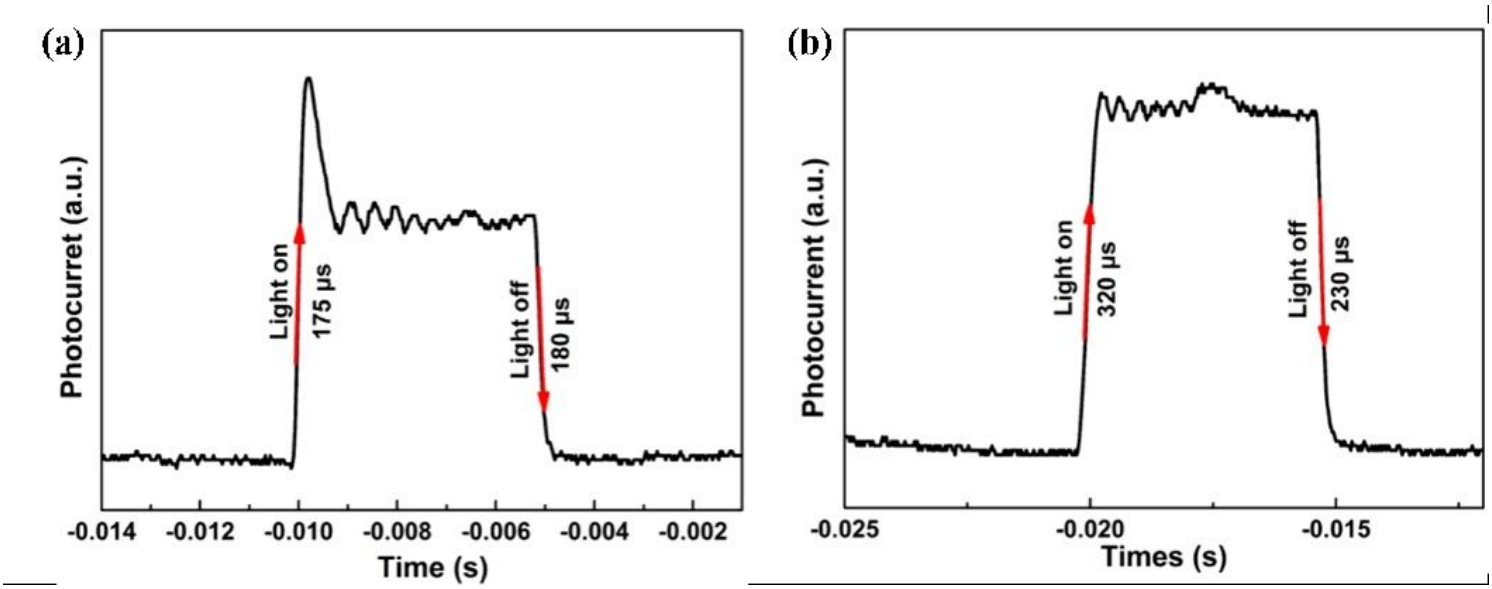

Figure 5

Response speed of CsPbIxBr3-x perovskite PDs. a CsPbI2Br perovskite photodetector, b CsPbIBr2 perovskite photodetector.

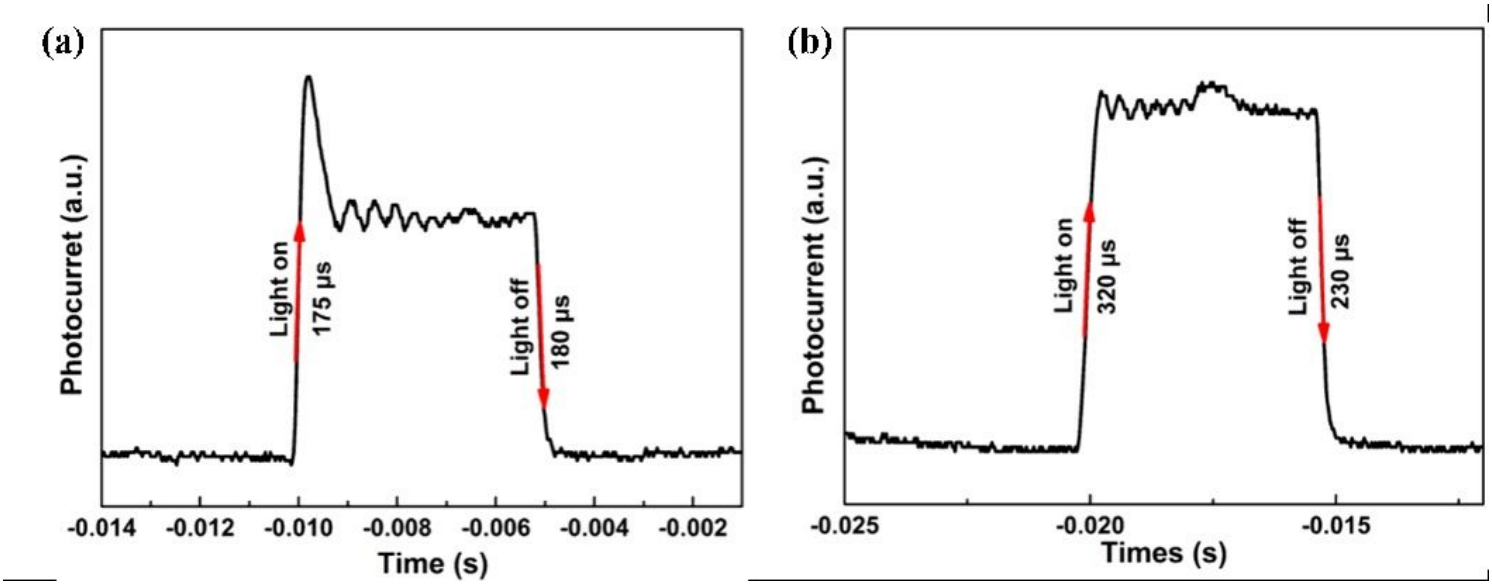

Figure 5

Response speed of CsPbIxBr3-x perovskite PDs. a CsPbI2Br perovskite photodetector, b CsPbIBr2 perovskite photodetector.